

Numerical and experimental study of SnO_x | Ag | SnO_x multilayer as indium-free transparent electrode for organic solar cells

Adrien Bou ^{a,b}, Philippe Torchio ^{a*}, Damien Barakel ^a, François Thierry ^a, Pierre-Yves Thoulon ^b and Marc Ricci ^b

^a Aix-Marseille Université, Institut Matériaux Microélectronique Nanosciences de Provence-IM2NP, CNRS-UMR 7334, Domaine Universitaire de Saint-Jérôme, Service 231, 13 397 Marseille Cedex 20, France

^b CROSSLUX, Immeuble CCE, Avenue Georges Vacher, ZI Rousset Peynier, 13 106 Rousset Cedex, France

ABSTRACT

We propose a SnO_x | Ag | SnO_x multilayer, deposited in a continuous vacuum atmosphere by E-beam evaporation, as transparent anode for a (poly-3-hexylthiophene):[6,6]-phenyl-C₆₁-butyric acid methyl ester (P3HT:PCBM) bulk heterojunction based Organic Solar Cell (OSC). Optical characterization of the deposited SnO_x is performed to determine the dispersion of the complex refractive index. A Transfer Matrix Method (TMM) numerical optimization of the thicknesses of each layer of the electrode is realized to limit the number of manufactured samples. A numerical study using the morphology of the silver inserted between the oxide layers as input data is performed with a Finite Difference Time Domain (FDTD) method to improve the accordance between measurement and optical model. Multilayers are manufactured with the objective to give to the electrode its best conductivity and transparency in the visible spectral range by using the results of the optical optimization. These bare tri-layer electrodes show low sheet resistance ($<10 \Omega/\square$) and mean transparency on [400-700] nm spectral band as high as 67 % for the whole Glass | SnO_x | Ag | SnO_x structure. The trilayer is then numerically studied inside a P3HT:PCBM bulk heterojunction based OSC structure. Intrinsic absorption inside the sole active layer is calculated giving the possibility to perform optical optimization on the intrinsic absorption efficiency inside the active area by considering the media embedding the electrodes.

Keywords: free-ITO electrode, oxide/metal/oxide, organic solar cell, optical optimization, TMM calculation, FDTD calculation, SnO_x , refractive index, thin silver layer.

1. INTRODUCTION

The sun gives us a massive renewable source of energy that can be collected in several ways. One of them is to convert the photons of the solar spectrum into electricity via a photovoltaic (PV) device. The possibilities of materials and structures to achieve such device are vast and until the last two decades were dominated by silicon and thin-film technologies. The production price and energy's cost of the crystalline silicon modules is currently high. Emerging PV devices as Organic Solar Cells (OSC) have the advantage of low manufacturing cost, high absorption coefficient and mechanical flexibility. Nevertheless, a weak absorption spectral band is associated to these alternative materials. Moreover, Indium Tin Oxide (ITO) is the most used transparent electrode for OSC, but Indium is highly employed and could become rare and expensive. Alternative to ITO is a substantial research field¹. One possibility are the multilayer

* philippe.torchio@univ-amu.fr, phone +33 (0) 4 91 28 83 49, fax +33 (0) 4 91 28 88 52, <http://www.im2np.fr/perso/torchio.html>

electrodes presenting an Oxide | Metal | Oxide structure²⁻⁸ that can give a transparent and conductive electrode with low sheet resistance and high transparency in a defined spectral range. In this paper, the numerical optimization⁹ of that kind of structure based on a SnO_x | Ag | SnO_x electrode¹⁰⁻¹² is investigated then manufactured.

2. SIMULATION AND EXPERIMENTAL

2.1 Simulation

An optical simulation through a Transfer Matrix Method (TMM) was performed. This method allows us to calculate the amplitude of the electromagnetic wave at each interface of a multilayer and to obtain the reflectance R , the transmittance T and the absorbance A of the stack. We have the possibility to calculate the absorption inside a single layer of the stack. This one-dimensional simulation method is rather fast to perform (less than one second for one calculation). A three-dimensional optical simulation was also performed by a Finite Difference Time Domain (FDTD) method^{9,13,14} which rigorously solves the Maxwell's equations and makes it possible to obtain the electromagnetic field versus time and position. This method requires more calculation time and memory space, but allows us to design three-dimensional structures.

The objectives of simulations are to be corroborated to the optical R , T and A measurements of Ag single layer, SnO_x single layer, and trilayer (figure 1) and to obtain the optimal transmission in a defined spectral range by varying the thicknesses of both SnO_x layer.

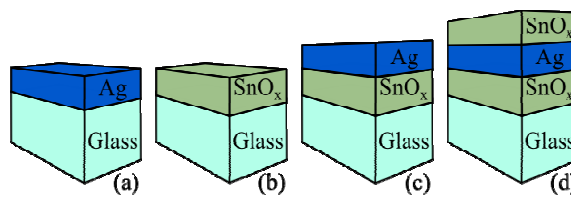


Figure 1 – (a) Schematics of thin Ag layer on glass – (b) to (d) Schematics of the different layers deposited on glass in order to build the transparent and conductive bare electrode.

In the TMM, a simple one-dimensional model (figure 2(a)) with effective complex refractive indices of Ag and SnO_x layer is used. In the FDTD method, we first replicate the TMM model design to make sure that the correspondences between both models are right. In a second step, we will still use measured complex refractive index of SnO_x and bulk refractive index of Ag, but also introduce its two-dimensional structure thanks to SEM images. This structured Ag layer is sandwiched between two SnO_x layers to obtain a more realistic three-dimensional model (figure 2(b)).

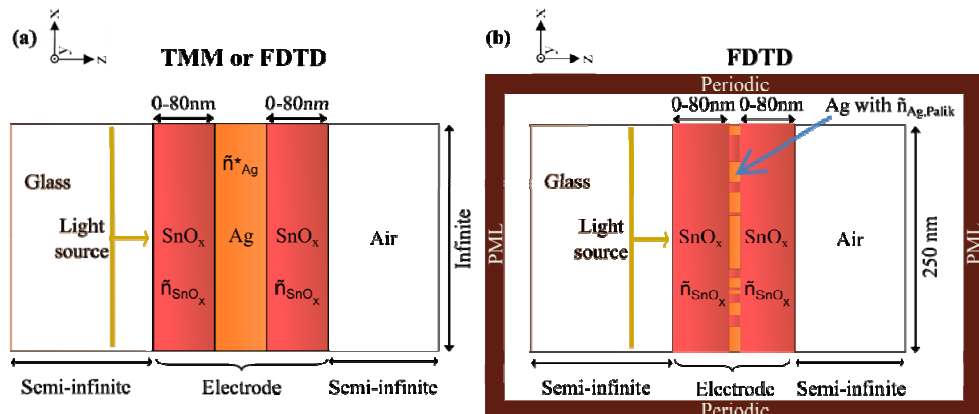


Figure 2 – (a) One-dimensional design for TMM or FDTD model – (b) Three-dimensional design for FDTD model

2.2 Experimental

Samples were prepared on cleaned VWR® cut edges plain glass slides measuring 76 x 26 mm² with a thickness of 1 mm. Substrates are presented into an Oerlikon Leybold Vacuum Univex 300 E-beam evaporator at normal incidence and with a distance of 20 cm from the liner containing the material to be deposited. The Ag thin film was deposited – from 99.99 % pure Ag into a 4cc Al₂O₃ liner both purchased from Neyco – at an average rate of 1.5 nm.s⁻¹ and a pressure around 2 x 10⁻⁵ mbar. The SnO_x layer was deposited – from 99.995 % pure SnO₂ into a 4cc Mo liner – at an average rate of 0.2 nm.s⁻¹ and a pressure around 1 x 10⁻⁴ mbar. The thickness is calibrated from a quartz crystal oscillator monitor placed near the substrate during the deposition then checked by a mechanical profilometer.

Samples are optically characterized by spectrophotometry including an integrating sphere. The absorption spectra (A=1-R-T) is deduced from measurements of R and T. A Carl Zeiss ULTRA® VP 40 Scanning Electron Microscope (SEM) was used to obtain images of silver morphology on glass and on SnO_x. The optical indices are measured with a GES5E SEMILAB Spectroscopic Ellipsometer.

Electrical measurements of sole Ag layer on glass, SnO_x | Ag bilayer and SnO_x | Ag | SnO_x trilayer are performed with a CPS Resistivity Test Fixture from CASCADE® combined with a C4S 4-Point Probe Head.

3. RESULTS

3.1 Experimental and numerical results with one-dimensional design for modeling (in air)

Spectroscopic ellipsometer measurements were performed to obtain the optical constants of around 30 nm SnO_x layer and 10 nm thick Ag layer deposited on glass (figure 3). With these values, we are able to calculate R, T and A for Glass | SnO_x | Ag | SnO_x structures using the one-dimensional design for TMM or FDTD method to compare numerical results to experimental measurements obtained from manufactured electrodes (figure 4). The mean absolute percentage error (MAPE) on T can be calculated from:

$$MAPE = \frac{1}{n} \sum_{i=1}^n \left| \frac{T_{i,\alpha} - T_{i,\beta}}{T_{i,\alpha}} \right| \quad (1)$$

where i is the i-th wavelength and n is the total number of measurement points (the same formula could be used for A and R by replacing T).

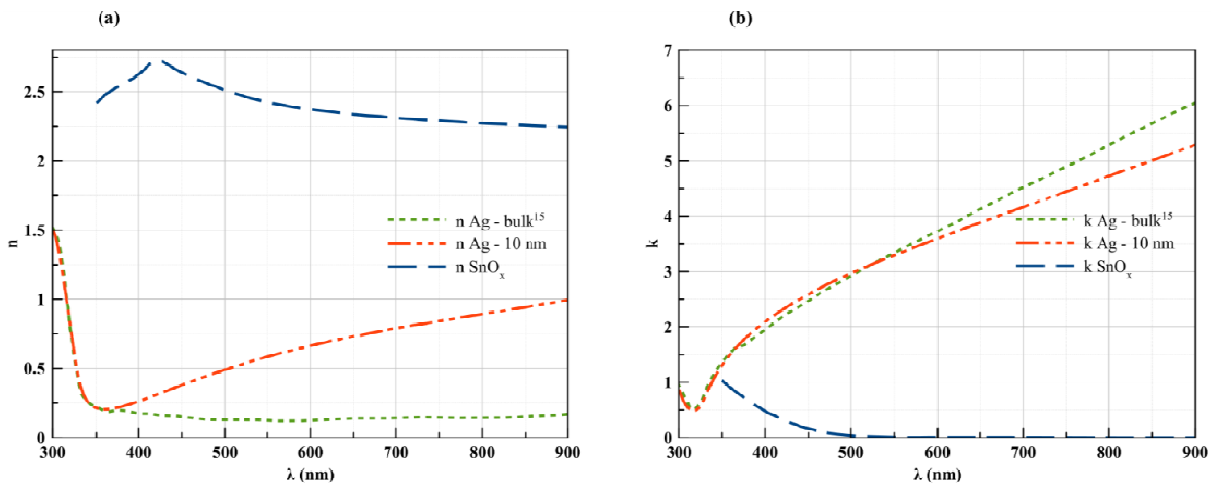


Figure 3 – (a) Bulk refractive index of Ag¹⁵ and measured refractive index of around 30 nm-thick SnO_x and 10 nm-thick Ag – (b) bulk extinction coefficient of Ag¹⁵ and measured extinction coefficient of around 30 nm-thick SnO_x and 10 nm-thick Ag.

The figure 4 presents the measured and calculated optical properties R, T and A versus wavelength for some selected oxide thicknesses. For numerical results, the values are corrected to take into account the first reflectance of the bare glass from outside (which not appeared in the figure 2(a)). We observe an agreement between both numerical models over the four different simulations presented in the figure 4 where averaged MAPE – α being then TMM result and β the FDTD result in the equation (1) – for R, T and A are respectively 9.3 %, 1.7 % and 3.6 %. These slight differences can be explained mainly by the way indices are taken into account in the model. In TMM model, indices are interpolated from ellipsometer experimental results while in the FDTD model, indices are fitted with a polynomial law. Moreover, we also note an agreement for different thicknesses of SnO_x layers in the trilayer for models and for the measurements of optical properties of the electrodes. The shapes of experimental R, T and A curves are in accordance with measurements. The MAPE values – α being then TMM result and β the measurements in the equation (1) – averaged over the four measured electrodes presented in the figure 4 are for R, T and A respectively 24.7 %, 7.5 % and 16.3 %. This allows us to validate our models and to proceed with numerical optimization.

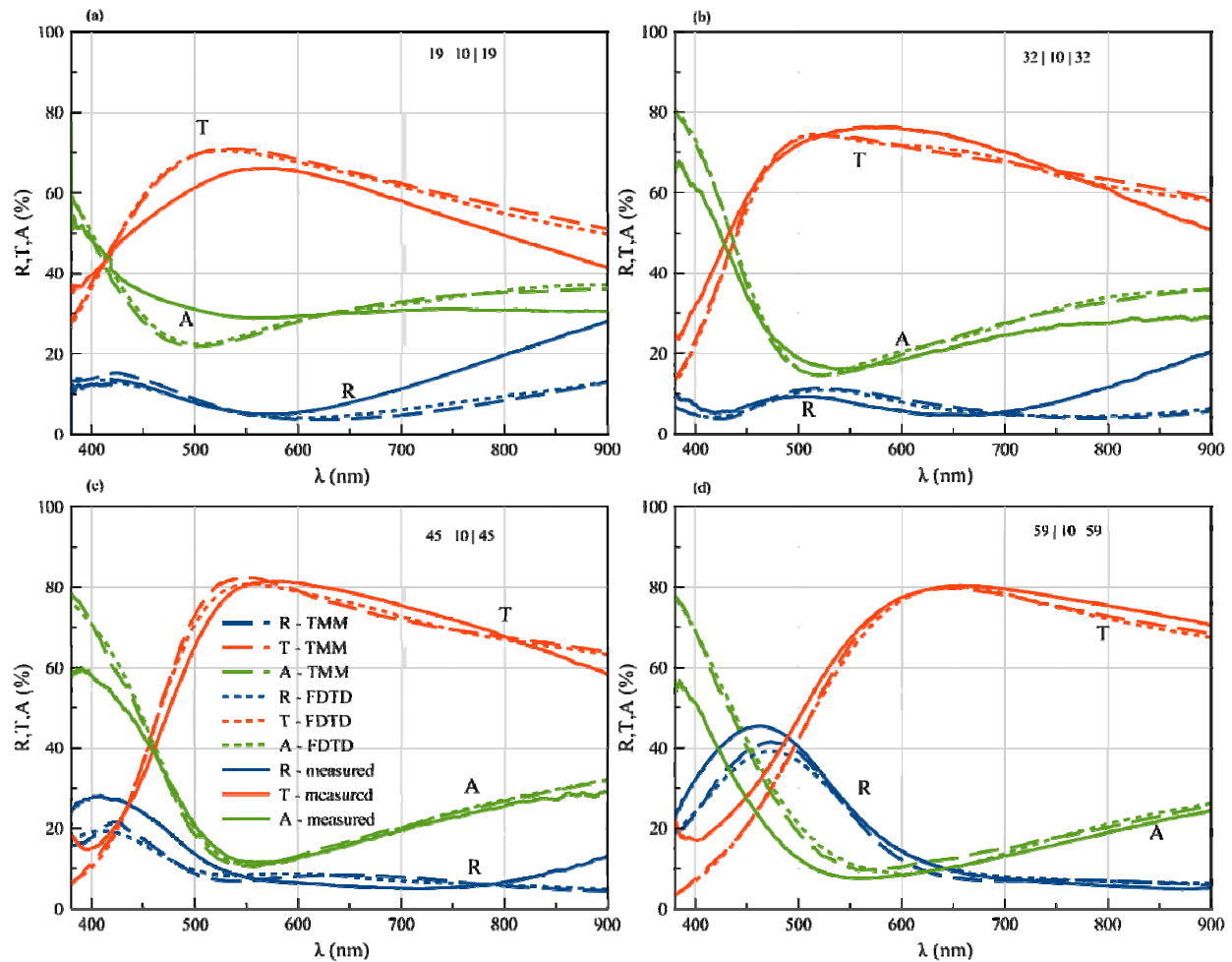


Figure 4 – Experimental and numerical transmittance T, reflectance R and absorptance A of (a) Glass | SnO_x (19 nm) | Ag (10 nm) | SnO_x (19 nm), (b) Glass | SnO_x (32 nm) | Ag (10 nm) | SnO_x (32 nm), (c) Glass | SnO_x (45 nm) | Ag (10 nm) | SnO_x (45 nm) and (d) Glass | SnO_x (59 nm) | Ag (10 nm) | SnO_x (59 nm).

In figure 5 is presented the cartography of the mean transmittance convoluted by the AM 1.5 solar spectrum in order to find the optimal thicknesses set of SnO_x layers of the electrode in air. This value is calculated from:

$$T_{ms} = \frac{\int_{\lambda_1}^{\lambda_2} I_{AM1.5}(\lambda) T(\lambda) d\lambda}{\int_{\lambda_1}^{\lambda_2} I_{AM1.5}(\lambda) d\lambda} \quad (2)$$

Both oxide layers' thicknesses are optimized in air by calculating T_{ms} in the considered [400-700] nm spectral band. We chose a variation step of 2 nm for x and y oxide thicknesses, ranging in the [0-80] nm scale. The Ag layer thickness remains fixed at 10 nm because it was proved to be a good compromise between high conductivity and high transparency for such trilayers.

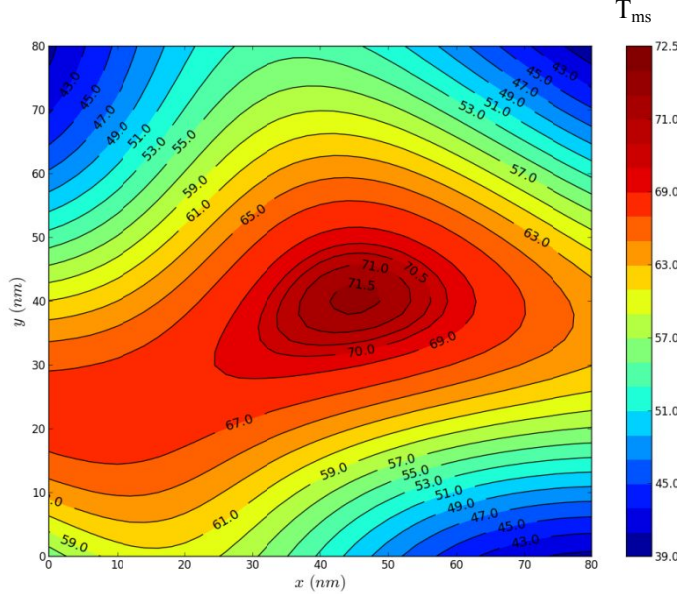


Figure 5 – Glass | SnO_x (x nm) | Ag (10 nm) | SnO_x (y nm) electrodes T_{ms} values for wavelengths ranging between 400 and 700 nm

$t_{\text{SnO}_x\text{-glass side}}$ (nm)	t_{Ag} (nm)	$t_{\text{SnO}_x\text{-air side}}$ (nm)	$T_{550}(\%)$	$T_{\text{mean}} (\%)$	$R_S (\Omega/\square)$	$\Phi_{T550} (\text{m}\Omega^{-1})$	$\Phi_{T\text{mean}} (\text{m}\Omega^{-1})$
19	10	19	65.8	59.5	16.1	0.95	0.34
19	10	59	58.6	53.9	17.5	0.27	0.12
30	10	30	73.5	63.6	15.3	3.00	0.71
32	10	32	75.8	65.4	14.5	4.32	0.99
40	10	53	75.6	65.8	16.4	3.72	0.93
45	10	45	80.7	64.0	10.7	10.9	1.08
45	10	45	78.5	61.7	6.7	13.3	1.19
45	10	45	74.8	66.6	11.5	4.58	1.49
53	10	40	80.4	66.9	18.0	6.27	1.00
59	10	59	67.2	58.1	17.3	1.09	0.25

Table 1 – Experimental transmittance at 550 nm and mean transmittance T_{mean} – for a wavelength between 400 and 700 nm –, sheet resistance R_S and factor of merit Φ_T of experimental trilayer SnO_x | Ag | SnO_x .

The arithmetic mean transmittance T_{mean} on a defined spectral range is calculated from:

$$T_{\text{mean}} = \frac{\int_{400 \text{ nm}}^{700 \text{ nm}} T(\lambda) d\lambda}{\int_{400 \text{ nm}}^{700 \text{ nm}} d\lambda} \quad (3)$$

The optimum structure in air is demonstrated to be Glass | SnO_x (44 nm) | Ag (10 nm) | SnO_x (40 nm), giving a 71.6 % T_{ms} value and 65.3 % mean transmittance T_{mean} for wavelengths ranging between 400 and 700 nm. Optical and electrical values of structures with other SnO_x thicknesses can be found in Table 1. This table provides the mean transmittance T_{mean} and the transmittance T_{550} at a wavelength of 550 nm, the sheet resistance R_s and the figures of merit Φ_{T550} and $\Phi_{T\text{mean}}$ of the manufactured electrodes. The figure of merit, proposed by G. Haake¹⁶, for transparent conductors is given by:

$$\Phi_T = \frac{T^{10}}{R_s} \quad (4)$$

The sheet resistance between 6 and 18 Ω/\square remains in the range of other similar efficient electrodes^{10,11}. The relatively low transparency of SnO_x for wavelengths under 500 nm leads to low transparency in this frequency domain for the trilayer too. Nevertheless, the remarkable agreement with simulation is a worthy start for this kind of structure, and the optimization of the deposition method of SnO_2 can be lead through a supply of oxygen flow. The strength of our simulation methods is to be also applied to other deposited materials.

3.2 Silver morphology for the three-dimensional design

The first consideration was to investigate the Ag structure at the surface of a glass substrate. The figure 6 presents SEM images of the silver percolation depending on the underlying layer. The surface is not completely covered by silver and reveals no isolated clusters. This morphology limits the Surface Plasmon Resonance (SPR) phenomenon which could increase absorption^{14,17,18}; but this permits a high conductivity of the Ag layer. The figure 6(a) shows a lower filling rate than those of the figures 6(b)-(c). On the figure 6(d), we do not observe clearly the structure of the silver at the surface of SnO_x . But such morphology can be introduced in our FDTD model for simulation. By using the E.D. Palik complex refractive index of silver¹⁵, a 3D-design can be simulated by FDTD (figure 2(b)) in air in order to compare results with experimental measurements and with the one-dimensional model (figure 7).

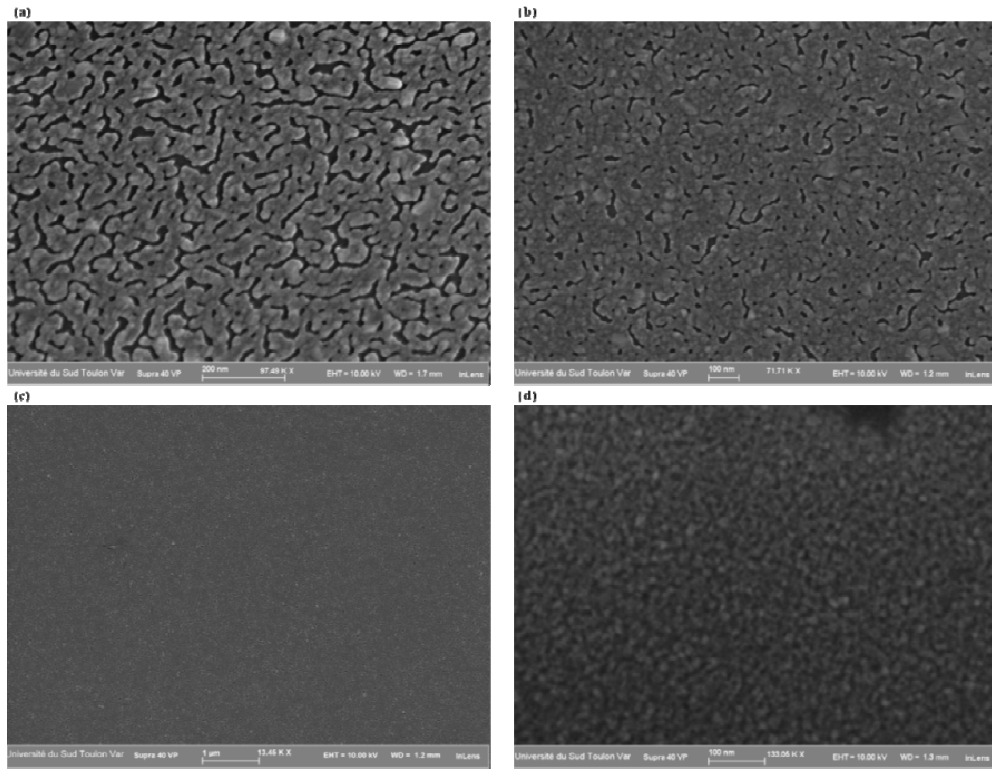


Figure 6 – SEM images showing the morphology of (a) 9 nm-thick Ag layer on glass, (b-c) 10 nm-thick Ag layer on glass (with two different scales) and (d) 10 nm-thick Ag layer deposited on 30 nm-thick SnO_x layer on a glass substrate.

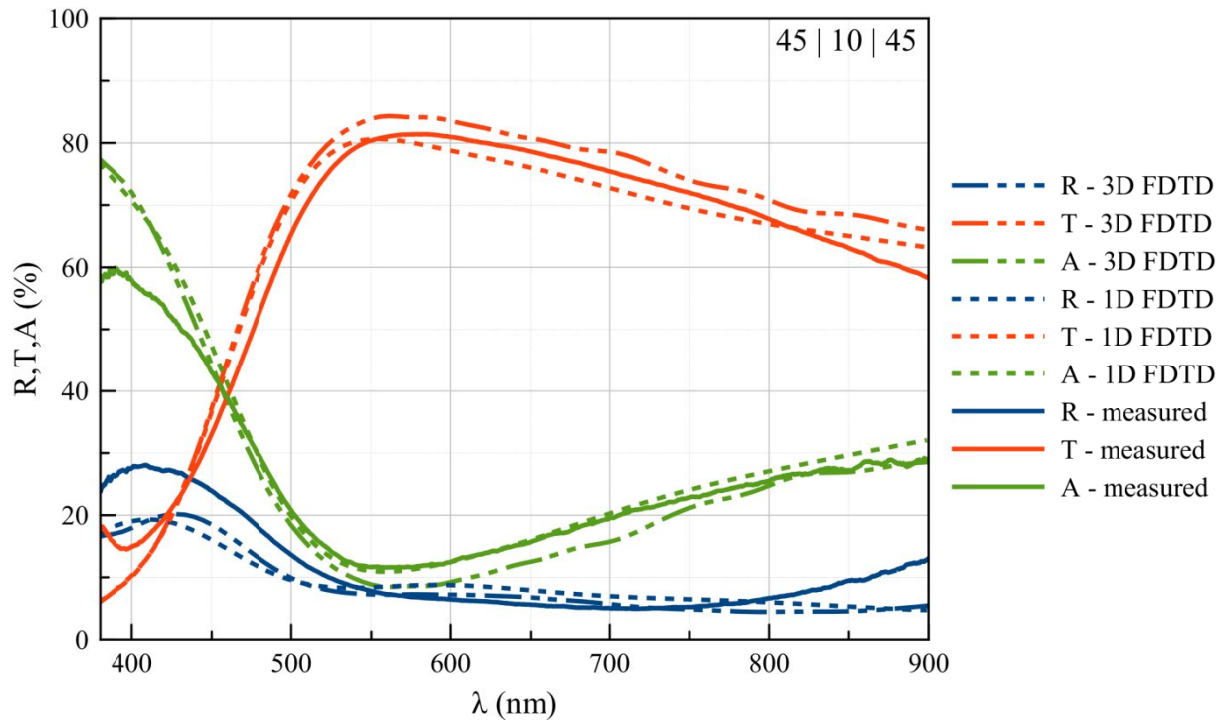


Figure 7 – Transmittance T, reflectance R and absorptance A of Glass | SnO_x (45 nm) | Ag (10 nm) | SnO_x (45 nm) of the three-dimensional design for FDTD model, the one-dimensional design for FDTD model and the experimental measurements.

The figure 7 shows the measured and calculated optical results for design presenting the best T₅₅₀ in table 1. The FDTD calculation relies on a three-dimensional design (figure 2(b)) which integrates a simulation zone for Ag of 250 nm² extracted from the center of the figure 6(b). An agreement is confirmed between the three-dimensional calculations and the experimental measurements. It is demonstrated that we can use SEM images to simulate the structure of Ag. Further work still need to be done with this three-dimensional design concept to improve the quality of the numerical transfer of SEM images and to approach to the experimental measurements.

3.3 One-dimensional design used for model in order to optimize a multilayer electrode as anode inside an OSC

Simulation can be applied to a whole organic solar cell. The main objective for PV-scientists should be to limit the manufacturing time by avoiding many production tests to find the optimal structure. For that, the intrinsic absorption efficiency in the active layer needs to be calculated from:

$$\eta_{A_{\text{active layer}}} = \frac{\int_{\lambda_1}^{\lambda_2} A_{\text{active layer}}(\lambda) I_{\text{AM1.5}}(\lambda) d\lambda}{\int_{\lambda_1}^{\lambda_2} I_{\text{AM1.5}}(\lambda) d\lambda} \quad (5)$$

Thus, a typical organic solar cell presenting the following design: Glass | SnO_x (x nm) | Ag (10 nm) | SnO_x (y nm) | PEDOT:PSS (50 nm) | P3HT:PCBM (180 nm) | Ag (100 nm), can be optimized to get the best $\eta_{A_{\text{active layer}}}$ by varying the thicknesses of both SnO_x layers in the [0-80] nm scale. We can then select the thicknesses which give the highest intrinsic absorption efficiency inside the active layer, i.e. P3HT:PCBM (figure 8).

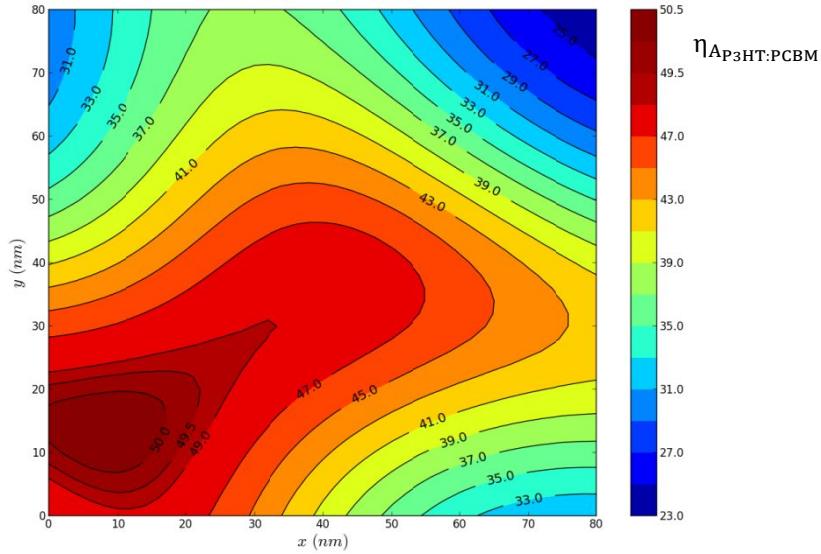


Figure 8 – Intrinsic absorption efficiency inside P3HT:PCBM for wavelengths between 350 and 660 nm for a Glass | SnO_x (x nm) | Ag (10 nm) | SnO_x (y nm) | PEDOT:PSS (50 nm) | P3HT:PCBM (180 nm) | Ag (100 nm) organic solar cell when varying the thicknesses of both SnO_x layers.

We obtain thinner optimal thicknesses for both oxides than in the optimization of the bare electrode in air - $x \approx 10$ nm and $y \approx 15$ nm. In this thickness domain - below 15 nm - we cannot be sure that the model is still accurate. As it can be seen in figure 4(a), the measured transmission is around 5 % below the simulated one.

4. CONCLUSION

In this paper, we present a numerical optimization method of trilayer transparent and conductive electrodes for OSC. An agreement is demonstrated between both manufactured and simulated electrodes. Experimental Glass | SnO_x | Ag | SnO_x electrodes show R_S as low as $6.7 \Omega/\square$ and T_{mean} (for wavelengths ranging between 400 and 700 nm) as high as 67 % taking in account R and A of the glass. Moreover, transparency increases up to a value of 80 % at the wavelength of 550 nm. The numerical optimization of a multilayer electrode as anode inside an OSC was done but needs to be corroborated with experimental results in the future.

ACKNOWLEDGEMENTS

The work presented in this paper was partially supported by the French Foundation of Technological Research (ANRT) under grant CIFRE-2012/0731.

REFERENCES

- [1] Granqvist, C.G., "Transparent conductors as solar energy materials: A panoramic review," *Solar Energy Materials and Solar Cells* 91(17), 1529–1598 (2007).
- [2] Cattin, L., Lare, Y., Makha, M., Fleury, M., Chandezon, F., Abachi, T., Morsli, M., Napo, K., Addou, M., et al., "Effect of the Ag deposition rate on the properties of conductive transparent $\text{MoO}_3/\text{Ag}/\text{MoO}_3$ multilayers," *Solar Energy Materials and Solar Cells* 117, 103–109 (2013).
- [3] Cattin, L., Morsli, M., Dahou, F., Abe, S.Y., Khelil, a., and Bernède, J.C., "Investigation of low resistance transparent $\text{MoO}_3/\text{Ag}/\text{MoO}_3$ multilayer and application as anode in organic solar cells," *Thin Solid Films* 518(16), 4560–4563 (2010).
- [4] Guillén, C., and Herrero, J., "TCO/metal/TCO structures for energy and flexible electronics," *Thin Solid Films* 520(1), 1–17 (2011).
- [5] Lopéz, I.P., Cattin, L., Nguyen, D.-T., Morsli, M., and Bernède, J.C., "Dielectric/metal/dielectric structures using copper as metal and MoO_3 as dielectric for use as transparent electrode," *Thin Solid Films* 520(20), 6419–6423 (2012).
- [6] Bernède, J.C., Cattin, L., Abachi, T., Lare, Y., Morsli, M., and Makha, M., "Use of Cu–Ag bi-layer films in oxide/metal/oxide transparent electrodes to widen their spectra of transmittance," *Materials Letters* 112, 187–189 (2013).
- [7] Nguyen, D.-T., Vedraine, S., Cattin, L., Torchio, P., Morsli, M., Flory, F., and Bernède, J.C., "Effect of the thickness of the MoO_3 layers on optical properties of $\text{MoO}_3/\text{Ag}/\text{MoO}_3$ multilayer structures," *Journal of Applied Physics* 112(6), 063505 (2012).
- [8] El Hajj, A., Lucas, B., Chakaroun, M., Antony, R., Ratier, B., and Aldissi, M., "Optimization of $\text{ZnO}/\text{Ag}/\text{ZnO}$ multilayer electrodes obtained by Ion Beam Sputtering for optoelectronic devices," *Thin Solid Films* 520(14), 4666–4668 (2012).
- [9] Vedraine, S., El Hajj, A., Torchio, P., and Lucas, B., "Optimized ITO-free tri-layer electrode for organic solar cells," *Organic Electronics* 14(4), 1122–1129 (2013).
- [10] Yang, J.-D., Cho, S.-H., Hong, T.-W., Son, D.I., Park, D.-H., Yoo, K.-H., and Choi, W.-K., "Organic photovoltaic cells fabricated on a $\text{SnO}_x/\text{Ag}/\text{SnO}_x$ multilayer transparent conducting electrode," *Thin Solid Films* 520(19), 6215–6220 (2012).
- [11] Yu, S.H., Jia, C.H., Zheng, H.W., Ding, L.H., and Zhang, W.F., "High quality transparent conductive $\text{SnO}_2/\text{Ag}/\text{SnO}_2$ tri-layer films deposited at room temperature by magnetron sputtering," *Materials Letters* 85, 68–70 (2012).
- [12] Kim, S.J., Stach, E. a., and Handwerker, C. a., "Silver layer instability in a $\text{SnO}_2/\text{Ag}/\text{SnO}_2$ trilayer on silicon," *Thin Solid Films* 520(19), 6189–6195 (2012).
- [13] Vedraine, S., Torchio, P., Duché, D., Flory, F., Simon, J.-J., Le Rouzo, J., and Escoubas, L., "Intrinsic absorption of plasmonic structures for organic solar cells," *Solar Energy Materials and Solar Cells* 95, S57–S64 (2011).
- [14] Vedraine, S., Torchio, P., Merlen, A., Bagierek, J., Flory, F., Sangar, A., and Escoubas, L., "Optical characterization of organic blend films integrating metallic nanoparticles," *Solar Energy Materials and Solar Cells* 102, 31–35 (2012).
- [15] Palik, E.D., "Handbook of Optical Constants of Solids," Elsevier Inc. Volume I, (1997).
- [16] Haacke, G., "New figure of merit for transparent conductors," *Journal of Applied Physics* 47(9), 4086 (1976).
- [17] Sangar, A., Merlen, A., Torchio, P., Vedraine, S., Flory, F., Escoubas, L., Patrone, L., Delafosse, G., Chevallier, V., et al., "Fabrication and characterization of large metallic nanodots arrays for organic thin film solar cells using anodic aluminum oxide templates," *Solar Energy Materials and Solar Cells* (2013).
- [18] Tabatabaei, M., Sangar, A., Kazemi-Zanjani, N., Torchio, P., Merlen, A., and Lagugné-Labarthet, F., "Optical Properties of Silver and Gold Tetrahedral Nanopyramid Arrays Prepared by Nanosphere Lithography," *The Journal of Physical Chemistry C* 117(28), 14778–14786 (2013).